nature publishing group

Fluorescence imaging of mitochondria in cultured skin fibroblasts: a useful method for the detection of oxidative phosphorylation defects

Boel De Paepe[1], Joél Smet[1], Arnaud Vanlander[1], Sara Seneca[2], Willy Lissens[2], Linda De Meirleir[2], Mado Vandewoestyne[3], Dieter Deforce[3], Richard J. Rodenburg[4] and Rudy Van Coster[1]

BACKGROUND: Protons are pumped from the mitochondrial matrix via oxidative phosphorylation (OXPHOS) into the intermembrane space, creating an electric membrane potential (ΔΨ) that is used for adenosine triphosphate (ATP) production. Defects in one or more of the OXPHOS complexes are associated with a variety of clinical symptoms, often making it difficult to pinpoint the causal mutation.

METHODS: In this article, a microscopic method for the quantitative evaluation of ΔΨ in cultured skin fibroblasts is described. The method using 5,5′,6,6′-tetraethylbenzimidazolyl-carbocyanine iodide (JC-1) fluorescence staining was tested in a selection of OXPHOS-deficient cell lines.

RESULTS: A significant reduction of ΔΨ was found in the cell lines of patients with either an isolated defect in complex I, II, or IV or a combined defect (complex I + complex IV). ΔΨ was not reduced in the fibroblasts of two patients with severe complex V deficiency. Addition of the complex I inhibitor rotenone induced a significant reduction of ΔΨ and perinuclear relocalization of the mitochondria. In cells with a heteroplasmic mitochondrial DNA (mtDNA) defect, a more heterogeneous reduction of ΔΨ was detected.

CONCLUSION: Our data show that imaging of ΔΨ in cultured skin fibroblasts is a useful method for the evaluation of OXPHOS functioning in cultured cell lines.

The majority of cellular adenosine triphosphate (ATP) is supplied in the mitochondria through oxidative phosphorylation (OXPHOS). The OXPHOS system consists of five multiprotein complexes embedded within the inner mitochondrial membrane: complex I (reduced nicotinamide adenine dinucleotide: ubiquinone oxidoreductase), complex II (succinate: ubiquinone oxidoreductase), complex III (ubiquinol: cytochrome c oxidoreductase), complex IV (cytochrome c oxidase), and complex V (ATP synthase). Complexes I, III, and IV pump protons, donated by reduced nicotinamide adenine dinucleotide, ubiquinone, and cytochrome c, respectively, into the mitochondrial intermembrane space. The proton gradient that develops between the mitochondrial matrix and the intermembrane space generates an electrochemical membrane potential (ΔΨ), which is the driving force for the conversion of ADP and inorganic phosphate into ATP (1).

The estimated incidence of OXPHOS defects in humans is ~1 in 5,000 live births. Isolated complex I deficiency (2) and the mitochondrial DNA (mtDNA) depletion syndromes (3) are the most commonly recognized mitochondrial disorders. Defects in OXPHOS are associated with a broad spectrum of symptoms and syndromes, ranging from mild myopathy to severe multisystem disorders. OXPHOS defects are complex due to the dual origin of genes involved and the specific nature of the mitochondrial genome. The mtDNA encodes 13 structural proteins of the complexes I, III, IV, and V; two rRNAs; and 22 transfer RNAs (tRNAs) necessary for intramitochondrial protein translation. The mitochondrial genome is polyploid, with multiple copies of mtDNA present within each individual mitochondrion. Two different populations of mtDNA can coexist within the same cell, wild type and mutant, a condition known as mtDNA heteroplasmy. Mitochondrial disease develops when the mutant load in a tissue exceeds the threshold above which the OXPHOS system is impaired. In addition to the 37 mtDNA genes, a multitude of nuclear genes are essential for proper functioning of the OXPHOS complexes. The latter encode structural OXPHOS components and a myriad of proteins involved in regulation, posttranslational modification, signaling, importation, folding, and assembly of the OXPHOS components (4).

Cultured skin fibroblasts are an attractive tissue for diagnostic testing of mitochondrial disease, considering the minimally invasive character of sampling and the large amount of cell material that can be obtained by culturing. In this study, we describe a microscopic method for quantification of the mitochondrial ΔΨ in cultured skin fibroblasts. We report the effect of preincubation with rotenone, a complex I inhibitor,

[1]Department of Pediatrics, Division of Pediatric Neurology and Metabolism, Ghent University Hospital, Ghent, Belgium; [2]Centre of Medical Genetics, Universitair Ziekenhuis Brussel, Vrije Universiteit Brussel, Brussels, Belgium; [3]Laboratory for Pharmaceutical Biotechnology, Ghent University, Ghent, Belgium; [4]Nijmegen Centre for Mitochondrial Disorders, Radboud University Nijmegen Medical Centre, Nijmegen, The Netherlands. Correspondence: Rudy Van Coster (rudy.vancoster@ugent.be)

Received 12 December 2011; accepted 08 May 2012; advance online publication 25 July 2012. doi:10.1038/pr.2012.84

on ΔΨ and evaluate the method by testing cells from patients harboring distinct OXPHOS deficiencies.

RESULTS

OXPHOS Complex I Inhibition

Mitochondria were visualized using the cationic dye 5,5′,6,6′-tetraethylbenzimidazolyl-carbocyanine iodide (JC-1), which indicates mitochondrial polarization by shifting its fluorescence emission from green to red through the formation of red fluorescent J-aggregates. To verify the viability of fibroblasts in culture, the percentage of apoptotic and necrotic cells was assessed in cell lines from control 1 (C1) to C5 and patient 2 (P2) to P6. It was found to be constant around 10%. No difference was seen between controls and patients (data not shown). A concentration range (10–60 ng/ml) of the complex I inhibitor rotenone was tested in two control and two patient cell lines for a fixed incubation period of 4 h at 37 °C. Cell lines were evaluated under the microscope and ΔΨ was quantified as relative red over green JC-1 fluorescence. A strong drop in ΔΨ was observed with 10 ng/ml of rotenone and inhibition remained at constant levels with up to 60 ng/ml of the inhibitor (Figure 1). Inhibitor concentrations higher than 30 ng/ml caused increasing cell death and loss of cellular adherence. On the basis of these observations, 30 ng/ml was chosen as an optimal rotenone concentration for further experiments. The rotenone regimen was tested for annexin-V binding, which revealed only a slight effect on cell death. In control fibroblast strains, average values of early apoptotic cells went from 1% in untreated to 2.5% in rotenone-treated cells, whereas necrotic or late apoptotic cells comprised 7.5 and 9%, respectively (Table 1). In our experimental setup, treatment with up to 6 mmol/l of the complex IV inhibitor potassium cyanide did not cause a detectable ΔΨ inhibition, whereas higher concentrations caused cell death (data not shown).

ΔΨ in Cultured Skin Fibroblasts From Controls and Patients

In control fibroblast cell lines, red JC-1 fluorescence predominated and was more abundant in the peripheral than in the perinuclear intracellular regions (Figure 2a). Rotenone treatment caused a decrease of red over green fluorescence and a condensation of mitochondria around the nucleus (Figure 2b). ΔΨ values similar to those from healthy controls were observed in cultured fibroblasts from a patient with mitofusin 2 mutation (P1). Evaluation of JC-1 fluorescence in cell lines from the patients with either an isolated OXPHOS deficiency or a combined OXPHOS deficiency (Figure 2c) showed a decrease of red over green fluorescence. Rotenone treatment made the heterogenic distribution of the defects apparent (Figure 2d–f). Subsequent immunostaining for complex IV subunit I showed a correlation between protein expression and preserved ΔΨ in P12 (Figure 2e, inset). In the patient with very low mtDNA mutation load (P13), the few fibroblasts with deficient ΔΨ had preserved complex IV immunoreactivity (Figure 2f, inset), showing that JC-1 is a more sensitive approach for picking up small reductions in mitochondrial function. The results of JC-1 fluorescence quantification in controls and patients are shown in Table 2. A graphic representation of grouped results in patients with OXPHOS deficiency is shown in Figure 3. The relative abundance of mitochondria with active ΔΨ, quantified as the red over green ratio, was significantly lower ($P = 0.00001$) in the patients with isolated OXPHOS complex I, II, and IV deficiencies (P2–7: 1.36 ± 0.24), as compared with healthy controls (C1–11: 2.31 ± 0.24). In contrast, the two patients with isolated OXPHOS complex V defect (P8–9) showed normal ΔΨ levels. ΔΨ levels were also significantly lower (1.40 ± 0.35, $P = 0.00003$) in the patients with a combined OXPHOS deficiency (P10–17), as compared with the controls. In control fibroblasts pretreated with the complex I inhibitor rotenone, ΔΨ values dropped 48 ± 12%. The rotenone-induced reduction of the ΔΨ in the patients with isolated OXPHOS complex I, II, and IV deficiency (P2–7, 57 ± 8%) was not significantly different from that in controls, but was significantly lower ($P = 0.00006$) in the patient group with combined OXPHOS defects (P10–17: 12 ± 16%).

Immunohistochemistry and Immunofluorescence

The ΔΨ-dependent fluorophore MitoTracker Red revealed alterations of the mitochondrial network in most of the patients with a heteroplasmic mtDNA mutation. An interruption of the mitochondrial network was observed, resulting in

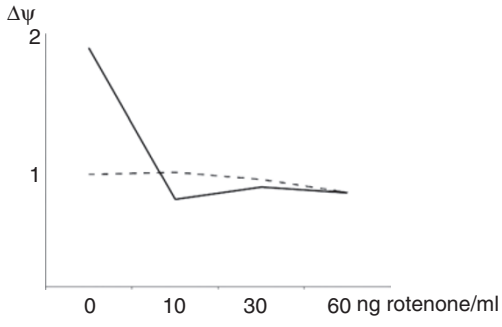

Figure 1. Effect of different rotenone concentrations on ΔΨ in cultured skin fibroblasts. Results of a representative experiment comparing control fibroblasts with oxidative phosphorylation-deficient fibroblasts: values for control 2 (black line) and patient 3 (dashed line) are given.

Table 1. Cell death in untreated versus rotenone-treated cultured skin fibroblasts

Cell line	C6		C7	
	Untreated	Rotenone-treated	Untreated	Rotenone-treated
Annexin V +	2	3	1	3
Annexin V and PI +	11	15	7	7
Total	123	149	117	88
Early apoptotic	2%	2%	1%	3%
Late apoptotic and necrotic	9%	10%	6%	8%

Cell death in fibroblasts exposed to 30 ng/ml of rotenone for 4 h. Early apoptotic cells were identified as annexin V positive, late apoptotic and necrotic cells as annexin V and propidium iodide (PI) double positive. Cultured fibroblasts from control patients C6 and C7 were tested.

a less tubular and more granular pattern in part of the cells (Figure 4b,c). This was not observed in fibroblasts from P13 and P16 (Figure 4d). In the two patients with complex V deficiency (P8, 9) and the patient with mtDNA depletion (P11), a more pronounced alteration of the mitochondrial architecture was seen. Several doughnut-shaped mitochondria were observed (Figure 4a). In six of eight patients with a combined OXPHOS deficiency (P10, 11, 12, 14, 15, and 17), a mosaic staining pattern of the fibroblasts was observed after immunofluorescent staining of the complex I subunit reduced nicotinamide adenine dinucleotide dehydrogenase ubiquinone Fe-S protein 7 (data not shown). Fibroblast cultures from P11, 12, and 14 also showed a mosaic staining pattern for complex IV subunit I. Cells lacking complex IV immunostaining maintained some residual ΔΨ, detected as low MitoTracker staining (Figure 4c). After preincubation with rotenone, a relocalization of the mitochondrial network toward the nucleus was seen (Figure 4h) as well as vimentin condensation (Figure 4f). The α-tubulin and β-actin staining remained unaltered. Perinuclear accumulation of the mitochondrial network was not seen after preincubation with potassium cyanide, an inhibitor of complex IV (data not shown).

Quantification of Mutated mtDNA in Patients With Mitochondrial Myopathy, Encephalopathy, Lactic Acidosis, and Stroke-Like Episode

We performed quantitative PCR to determine the mtDNA mutation load in the cultured skin fibroblasts from two patients with mitochondrial myopathy, encephalopathy, lactic acidosis, and stroke-like episodes (MELAS) carrying the m.3243A→G mutation. The total mutation load was 46.4 and 55.8% in P16 and P17, respectively. In fibroblasts from the same passage,

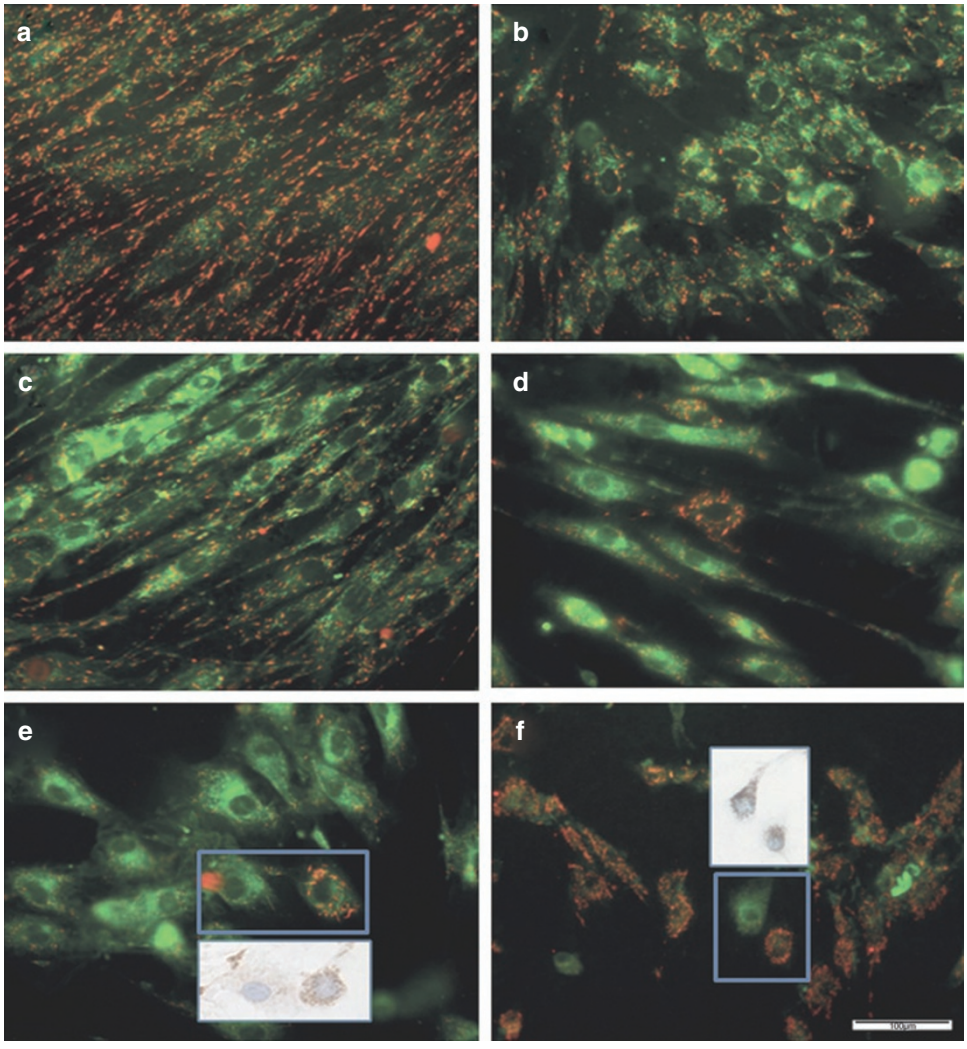

Figure 2. 5,5′,6,6′-Tetraethylbenzimidazolyl-carbocyanine iodide (JC-1) staining in cultured skin fibroblasts. (**a,b**) Control: red and green JC-1 staining in (**a**) untreated and (**b**) rotenone-treated fibroblasts. (**c–e**) Patient 12: red and green JC-1 staining in (**c**) untreated and (**d**) rotenone-treated fibroblasts. Red and green JC-1 staining in (**e**) rotenone-treated fibroblasts, with inset showing subsequent immunostaining for oxidative phosphorylation (OXPHOS) complex IV subunit I (3,3′-diaminobenzidine + chromogen, brown). Note the correlation between preserved electrochemical membrane potential (ΔΨ) and OXPHOS protein. (**f**) Patient 13: red and green JC-1 staining in rotenone-treated fibroblasts, with inset showing subsequent immunostaining for OXPHOS complex IV subunit I (3-3′-diaminobenzidine, brown). Note that the rare fibroblasts with failed ΔΨ have preserved OXPHOS protein immunoreactivity. Bar = 100 µm.

Table 2. Relative red over green 5,5′,6,6′-tetraethylbenzimidazolyl-carbocyanine iodide fluorescence

Number	Untreated	Rotenone-treated	Number	Untreated	Rotenone-treated
C1	2.48 ± 0.16	0.90 ± 0.09	P4	1.67 ± 0.36	0.64 ± 0.14
C2	2.08 ± 0.11	0.87 ± 0.19	P5	1.29 ± 0.22	0.74 ± 0.30
C3	2.36 ± 0.17	1.28 ± 0.17	P6	1.58 ± 0.10	0.69 ± 0.08
C4	2.62 ± 0.47	1.42 ± 0.11	P7	1.35 ± 0.32	0.81 ± 0.06
C5	2.28 ± 0.36	0.89 ± 0.17	P8	2.58 ± 0.51	0.56 ± 0.11
C6	2.16 ± 0.13	0.81 ± 0.07	P9	2.65 ± 0.39	0.92 ± 0.07
C7	2.25 ± 0.12	1.50 ± 0.10	P10	1.47 ± 0.48	1.38 ± 0.35
C8	2.12 ± 0.41	0.91 ± 0.15	P11	1.69 ± 0.52	1.27 ± 0.31
C9	2.18 ± 0.25	1.50 ± 0.21	P12	0.87 ± 0.27	0.97 ± 0.26
C10	2.81 ± 0.53	1.12 ± 0.22	P13	1.64 ± 0.31	1.39 ± 0.31
C11	2.06 ± 0.01	0.87 ± 0.13	P14	1.12 ± 0.35	1.19 ± 0.28
P1	2.29 ± 0.35	1.37 ± 0.16	P15	1.33 ± 0.14	1.22 ± 0.30
P2	1.00 ± 0.20	0.94 ± 0.14	P16	1.94 ± 0.33	1.24 ± 0.41
P3	1.28 ± 0.33	0.81 ± 0.10	P17	1.49 ± 0.26	1.16 ± 0.22

Relative mean values of 10 microscopic fields ± SD are given, both in untreated fibroblasts and in fibroblasts pretreated for 4 h with 30 ng/ml of rotenone. C, control; P, patient.

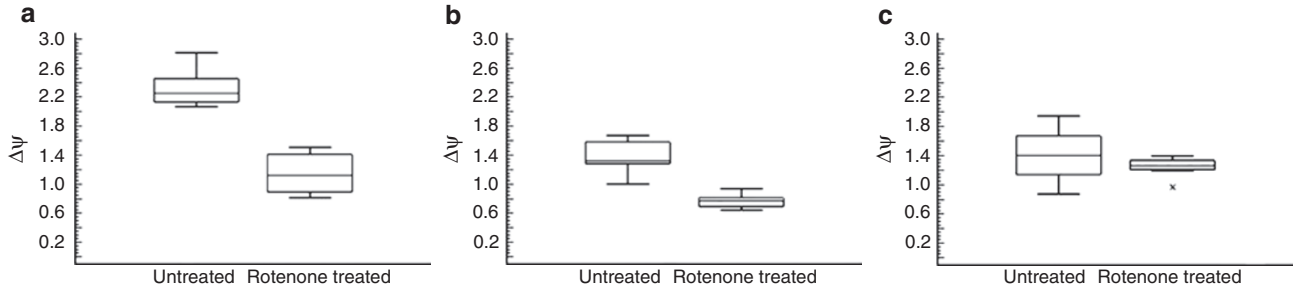

Figure 3. Box plots of 5,5′,6,6′-tetraethylbenzimidazolyl-carbocyanine iodide (JC-1) fluorescence quantification in skin fibroblasts. Comparison of relative red over green JC-1 fluorescence (ΔΨ) in (**a**) controls 1–11, with (**b**) patients harboring isolated complex I, II, and IV defects (patients 2–7) and (**c**) patients with combined complex I and IV defects (patients 10–17), in untreated and rotenone-treated fibroblasts. The *x* value in panel **c** represents an outlier smaller than the lower quartile minus three times the interquartile range.

single-cell PCR was performed to study the distribution of the mtDNA mutations in individual cells. Fifty cells of each patient were laser captured, of which 21 (P16) and 24 (P17) could be reliably scored for mutation load. Analysis showed substantial segregation of the defect between individual cells (Figure 5). In the fibroblasts of P16, the majority of the cells had undetectable levels of mutated mtDNA (Figure 5a), which could explain the mild reduction of overall ΔΨ in this cell line.

DISCUSSION

ΔΨ Is Compromised in Cultured Skin Fibroblasts From Patients With Defects in the OXPHOS Complexes I, II, and IV

In the pilot study presented here, JC-1 staining was used for monitoring the mitochondrial membrane potential in cultured skin fibroblasts from 16 patients with OXPHOS deficiency. A method for quantification of the JC-1 fluorescent emissions is described. In the fibroblasts from the patients with an isolated deficiency of complex I, complex II, or complex IV and from the patients with a combined OXPHOS complex deficiency (complex I + IV), a significant reduction of ΔΨ was observed. In contrast, cultured skin fibroblasts from the patients with isolated complex V deficiency had a normal ΔΨ. Unmistakably, an OXPHOS deficiency potentially disturbs the build-up of ΔΨ. Our results confirm earlier findings of a reduced mitochondrial membrane potential in cultured skin fibroblasts from three patients with complex I deficiency. Willems *et al.* quantified the tetramethylrhodamine methyl ester fluorescence in one patient with nuclear NDUFS4 mutation and found a slight but significant decrease of ΔΨ (5). Similar reductions of tetramethylrhodamine methyl ester fluorescence were observed in cultured skin fibroblasts from two patients with mutations in other structural subunits of complex I (NDUFS7 and NDUFS8) (6). In line with our results, a preserved ΔΨ was observed in cultured skin fibroblasts from a patient with the heteroplasmic m.9176T→G mutation in the mitochondrial *ATP6* gene encoding subunit a of complex V (7).

Rotenone Inhibits ΔΨ and Causes Intracellular Rearrangements

Preincubation of control fibroblasts with the complex I inhibitor rotenone significantly decreased ΔΨ. Rotenone disrupts the electron transfer in complex I between the terminal FeS cluster and ubiquinone and inhibits, in this

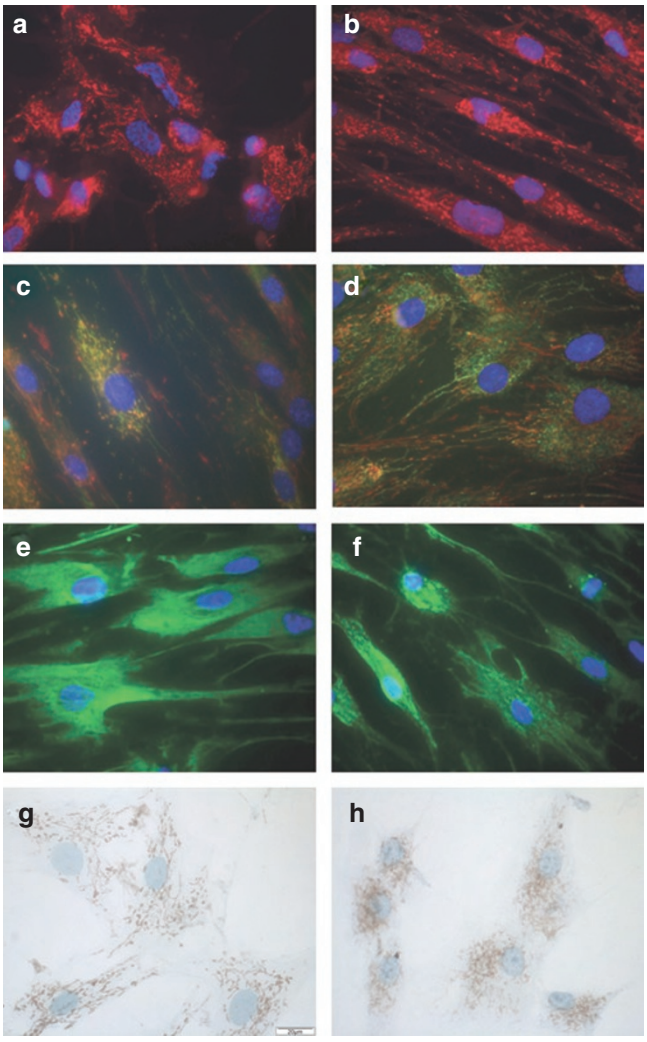

Figure 4. MitoTracker, immunofluorescent and immunocytochemical staining in cultured skin fibroblasts. (**a**) Patient 8: MitoTracker (red) staining shows aberrant mitochondrial morphology and distribution in fibroblasts with complex V deficiency. (**b**) Patient 17: MitoTracker (red) staining shows a granular staining pattern in fibroblasts from a patient with mitochondrial myopathy, encephalopathy, lactic acidosis, and stroke-like episodes. The distribution pattern, stretching to the periphery of the cells, is preserved. (**c**) Patient 12: double fluorescent staining with MitoTracker (red) and an antibody against complex IV subunit I (AlexaFluor green) in fibroblasts from a patient with a heteroplasmic mtDNA $tRNA^{Lys}$ mutation showing low oxidative phosphorylation (OXPHOS) staining and rare colocalization (yellow). (**d**) Patient 13: double fluorescent staining with MitoTracker (red) and an antibody against complex IV subunit I (AlexaFluor green) in fibroblasts from a patient with a heteroplasmic mtDNA $tRNA^{Asp}$ mutation showing preserved OXPHOS staining. (**e,f**) Control: normal vimentin staining pattern (AlexaFluor green) in untreated cells (**e**) and condensation of vimentin in rotenone-treated cells (**f**). (**g,h**) Patient 13: the tubular OXPHOS complex IV subunit I staining pattern (3-3′-diaminobenzidine, brown) of untreated cells (**g**) is lost in rotenone-treated cells, which show perinuclear reorganization of mitochondria (**h**). Bar = 20 µm.

Table 3. Patient information

Patient	Gender/ age	Clinical features	Causal mutation	Reference
P1	M/36	Charcot-Marie-Tooth	Mitofusin 2 (heterozygous p.Arg94Trp)	
P2	F/14	Cardiomyopathy	ND	
P3	F/<1	Failure to thrive, microcephaly	NDUFS4 (homozygous p.Trp96 Stop)	5
P4	M/1	Encephalopathy, psychomotor retardation	ND	
P5	F/<1	Leigh syndrome	NDUFS4 (homozygous p.Arg106 Nonsense)	
P6	F/<1	Leigh syndrome	Fp (homozygous p.Gly555Glu)	6
P7	F/3	Leigh syndrome	SURF-1 (homozygous c.312_321del insAT)	
P8	M/20	Epilepsy, mild mental retardation	TMEM70 (compound heterozygous c.251delC/c.317-2A→G)	
P9	M/<1	Infantile lactic acidosis	ATP12 (homozygous p.Trp94Arg)	7
P10	F/18	Cardiomyopathy	ND	
P11	F/3	Hepatopathy, myopathy	POLG (heterozygous p.Ala467Thr p.Leu860Arg)	
P12	F/<1	Leigh syndrome	$tRNA^{Lys}$ (95% m.8344A→G)	8
P13	F/17	Myopathy	$tRNA^{Asp}$ (<3% m.7526A→G)	9
P14	M/<1	Nephro-encephalo-myopathy	$tRNA^{Asn}$ (50% m.5728A→G)	10
P15	F/<1	Hypotonia, hyperlactatemia	$tRNA^{Glu}$ (91% m.14709T→C)	11
P16	F/3	MELAS	$tRNA^{Leu}$ (46% m.3243A→G)	
P17	F/67	MELAS	$tRNA^{Leu}$ (55% m.3243A→G)	

F, female; M, male; MELAS, mitochondrial myopathy, encephalopathy, lactic acidosis and stroke-like episodes; ND, not determined; tRNA, transfer RNA.

way, the proton pumping from the matrix into the intermembrane space. A similar reduction of $\Delta\Psi$ was observed in rotenone-subjected cells from controls and from patients with isolated complex I, II, or IV deficiency. However, cells from patients with combined complex I and IV deficiency appeared more resistant to rotenone inhibition, a feature that can potentially differentiate them from cells with isolated OXPHOS defects.

Not only was a decrease of $\Delta\Psi$ seen after rotenone treatment, but, surprisingly, morphological changes of the mitochondrial network were also observed. The mitochondria became more clustered around the nucleus. Mitochondria are dynamic organelles that have intimate contacts with other cellular

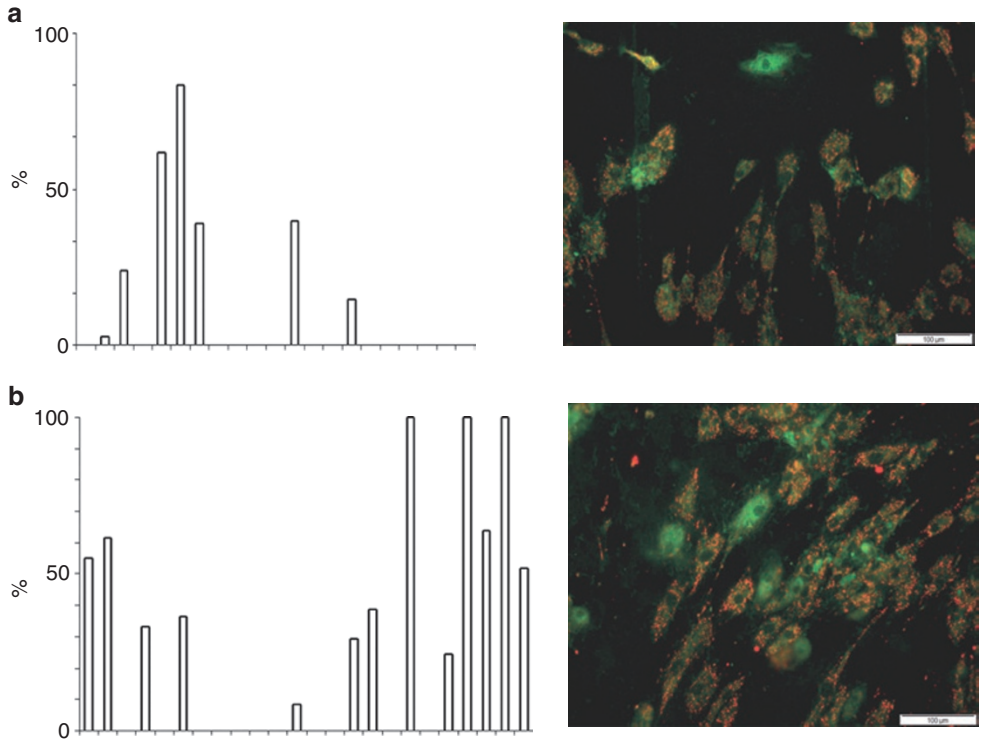

Figure 5. Percentages of mutated mtDNA and 5,5′,6,6′-tetraethylbenzimidazolyl-carbocyanine iodide (JC-1) fluorescent images in individual cultured skin fibroblasts from patients with mitochondrial myopathy, encephalopathy, lactic acidosis and stroke-like episodes. Graphs depict the percentage of the $tRNA^{Leu}$ A3243G mutation as determined by single-cell PCR in (**a**) patient 16 and (**b**) patient 17 in 21 and 24 cells, respectively. Representative JC-1 fluorescent images are shown alongside. Bar = 100 µm.

structures such as the nucleus, endoplasmic reticulum, Golgi, and cytoskeleton (8). We showed that the rotenone-induced perinuclear clustering of mitochondria was accompanied by alterations of the vimentin network. In contrast, microfilaments and microtubules remained unchanged after preincubation with the complex I inhibitor. Earlier reports in the literature have also shown that the addition of rotenone was linked to cytoskeletal changes, but some controversy remains. Some authors suggest that the complex I inhibitor disturbs the organization of the microtubules (9,10). Accumulating evidence, however, supports an association of the mitochondria with intermediate filaments rather than with microtubuli. One argument is that in various cell lines, intermediate filaments are enriched in the mitochondrial fraction and coimmunoprecipitate with intact mitochondria (11). In addition, a disturbed intermediate filament network was found in myoblasts from the patients with the heteroplasmic m.3243A→G mutation (12), and in cultured skin fibroblasts from the patients with the m.5650G→A mutation in the mitochondrial $tRNA^{Ala}$ gene (13). In these studies, the distribution of actin and α-tubulin was unchanged. Nonetheless, we and others (14) could not show that OXPHOS deficiency as such causes perinuclear clustering of mitochondria the fibroblasts of patients, which argues against OXPHOS deficiency in itself being the prerequisite for perinuclear relocalization of mitochondria. It remains elusive whether rotenone induces cytoskeletal changes indirectly, through inhibition of the ΔΨ, or directly through an interaction with the intermediate filaments.

Heterogeneous OXPHOS Defects Are Detected With Fluorescent Microscopy

In the past, ΔΨ was most often quantified by measuring JC-1 emission at 520 and 595 nm using a microplate reader. Using such an approach, the cell culture is studied as a whole and evaluation of individual cells is not possible. When such a method is used for the study of heterogeneous mitochondrial defects, differences between individual cells cannot be observed and patients with a low mutation load will be missed. The method described here is ideally suited for the detection of patients with heterogeneously distributed defects, including heteroplasmic mtDNA mutations and mtDNA depletion. In these patients, the OXPHOS defect can vary significantly from cell to cell. When subjected to rotenone, mitochondria condensate around the nucleus, which substantially aids the visualization of fibroblasts with preserved ΔΨ. By this technique, heterogeneities in the culture are accentuated, which allows the identification of individual cells with either high or low mutation load.

Following fluorescence imaging of the mitochondrial ΔΨ, proteins can be subsequently visualized by immunocytochemistry. Sequential JC-1 and OXPHOS immunostaining in fibroblasts from a patient with myoclonic epilepsy and ragged-red fibers mutation allowed us to show a correlation between maintained ΔΨ and preserved OXPHOS immunoreactivity. We further dissected the variation between individual fibroblasts through single-cell PCR in two patients with MELAS and showed a remarkable degree of variation

Table 4. Oxidative phosphorylation results in patient tissues

Patient	Cultured skin fibroblasts			Skeletal muscle		
	Spectrophotometry (II, III, and IV)	BN PAGE	Immunocytochemistry	Spectrophotometry (I, II, III, IV, and V)	BN PAGE	Immunohistochemistry
P1	Normal	ND	ND	ND	ND	ND
P2	Normal	ND	Low complex I	Low complex I	Low complex I	ND
P3	Low complex III	Low complex I and III	Normal	Low complex I	Low complex I	ND
P4	Normal	Low complex I	ND	Low complex I	Low complex I	ND
P5	Normal	Low complex I	Low complex I	Low complex I	Low complex I	ND
P6	Low complex II	Low complex II	Normal	Low complex II	ND	ND
P7	Low complex IV	Low complex IV	Low complex IV	Low complex IV	Low complex IV	ND
P8	Normal	Low complex V	Low complex V	Low complex I and III	Low complex V	ND
P9	ND	Low complex V	Low complex V	Normal	Low complex V	Normal
P10	Normal	Low complex I	Low complex I	Low complex I and IV	ND	ND
P11	Normal	Low complex IV, V subcomplexes	Complex I and IV mosaic staining	ND	ND	ND
P12	Normal	Low complex I and IV	Complex I and IV mosaic staining	Normal	ND	Complex I and IV mosaic staining
P13	Normal	Normal	Low complex I	Low complex I and IV	ND	ND
P14	Low complex IV	Normal	Complex I mosaic staining	Low complex I and IV	Low complex I, V subcomplexes	ND
P15	Normal	Low complex I and IV	Complex I mosaic	ND	Low complex I and IV	ND
P16	Normal	ND	Normal	Normal	ND	ND
P17	ND	ND	Complex I mosaic staining	Low complex I	ND	ND

BN PAGE, blue native-polyacrylamide gel electrophoresis; ND, not determined.

of the $tRNA^{Leu}$ m.3243A→G mutation load among cells. This intriguing phenomenon has been reported earlier in a patient with neuropathy ataxia retinitis pigmentosa with m.8993T→G mutation in the mitochondrial *MTATP6* gene. In this patient, the peripheral blood lymphocytes (30 cells tested) had an overall mutation load of 44% but displayed a wide range of variation. Four cells even contained no mutant mtDNA (15). The strong variation of mutation load has also been reported in blood cells and metaphase II oocytes and their respective polar bodies in women with heteroplasmic m.3243A→G $tRNA^{Leu}$ mutation (16). The two fibroblast cell lines from patients with MELAS studied here also showed differences in mutation segregation, resulting in a large number of defect-free cells in one cell line. This could explain why the mitochondrial function is much less compromised in that particular cell line. Linear regression analysis revealed no significant correlation between the average mutation load and ΔΨ values in the six cell lines with heteroplasmic tRNA mutations ($R^2 = 0.36$, $P = 0.2$), which is an additional clue that mitochondrial dysfunction is strongly dependent upon the cell-to-cell distribution of the gene defect. Our observations emphasize the complexity of heteroplasmic mtDNA defects and stress the importance of visualizing OXPHOS defects at the cellular level.

In conclusion, our data further substantiate the relevance of testing skin-derived fibroblasts for diagnosing OXPHOS defects. The reported JC-1 microscopic approach provides a convenient method for the detection of a deficiency of complex I, II, and IV through ΔΨ reduction and allows quantification using image analysis. In addition, JC-1 fluorescent staining of rotenone-treated fibroblasts is particularly suited for visualizing heteroplasmic OXPHOS defects.

METHODS

Patients and Cell Lines

Fibroblast cell cultures were derived from a diagnostic skin biopsy. Ethical approval was obtained from the Ghent University Institutional Review Board, and all patients or patients' guardians signed an informed consent. Control fibroblasts were obtained from patients in whom evidence of neither a mitochondrial nor other neurological disease was found.

Patient information is listed in Table 3 (17–23). Diagnostic workup of the cultured skin fibroblasts consisted of spectrophotometric analysis of the activities of complex II (24), III (25), and IV (26) and activity staining of all complexes after separation by blue native-polyacrylamide gel electrophoresis (27) and immunocytochemical staining (28) (Table 4). On the basis of the results obtained in skeletal muscle and other tissues, subjects were subdivided into patients with isolated OXPHOS defects and those with combined complex I and IV deficiency. Fibroblasts were grown in Earle's Salts 199 medium (PAA Laboratories, Linz, Austria) supplemented with 20% fetal bovine serum, 0.5 U/ml penicillin–streptomycin, and 1% kanamycine (Invitrogen, Carlsbad, CA) in a humidified incubator with 5% CO_2 at 37 °C. For microscopy, fibroblasts were grown on glass chamber slides (Nunc, Rochester, NY) until a confluence range of 60–80% was reached.

Viability of Cell Lines

To identify apoptotic cells in the cultures, cells were stained using the ApoTarget kit (Invitrogen) according to the manufacturer's instructions. Live fibroblasts were visualized under a fluorescence microscope (Carl Zeiss, Goettingen, Germany), identifying early apoptotic cells as annexin V–fluorescein isothiocyanate positive and late apoptotic or necrotic cells as annexin V–fluorescein isothiocyanate and propidium iodide double positive. A minimum of 75 cells was scored per patient, and mean values and SD were calculated. Differences were considered statistically significant when Student's *t*-tests gave P values < 0.05.

JC-1 Fluorescent Staining

Fibroblasts were either treated with a single dose of rotenone dissolved in ethanol for 4 h at 37 °C or the same volume of solvent. Cells were washed with phosphate-buffered saline. An amount of 5 μg/ml of 5,5′,6,6′-tetraethylbenzimidazolyl-carbocyanine iodide (JC-1; Invitrogen) was added, and the cells were incubated for 30 min at 37 °C. After three successive washes with phosphate-buffered saline for 5 min each, live fibroblasts were visualized under a fluorescence microscope (Olympus, Hamburg, Germany), detecting red and green fluorescent emission separately using optical filters (29). JC-1 staining is a quantitative indicator of $\Delta\Psi$ (30). We quantified red over green JC-1 fluorescence ratios by converting images to bright field and measuring the average grayscale (Cell F software; Olympus). Ten microscopic fields ×400 magnification selected at random, typically containing between 50 and 100 cells, were measured per chamber. Mean values and SDs were calculated. Differences were considered statistically significant when Student's *t*-tests gave P values < 0.05.

Immunocytochemical Staining

Slides were immunostained according to published procedures (28). Briefly, acetone-fixed fibroblasts were stained with a monoclonal antibody directed against complex IV subunit I (3 μg/ml, MitoSciences, Eugene, OR) visualized with the LSAB2 kit (Dako, Glostrup, Denmark) and 3,3′-diaminobenzidine + chromogen (Dako). Cell nuclei were counterstained with hematoxylin Gill number 2 (Sigma-Aldrich, St Louis, MO).

MitoTracker and Immunofluorescent Staining

Fibroblasts were incubated with 25 ng/ml MitoTracker Red CMXRos (Invitrogen), a selective fluorescent dye for active mitochondria, for 45 min at 37 °C, after which the cells were fixed in 3.5% paraformaldehyde for 15 min at 37 °C and permeabilized for 3 min in ice-cold acetone. Slides were blocked with 2.5% bovine serum albumin in phosphate-buffered saline for 30 min. Subsequently, slides were incubated with monoclonal antibodies directed against OXPHOS complex I subunit NDUFS7 (2 μg/ml, MitoSciences) or complex IV subunit I (2 μg/ml, MitoSciences), β-actin (1 μg/ml, Santa Cruz Biotechnology, Santa Cruz, CA), vimentin (0.7 μg/ml, Invitrogen), and α-tubulin (5 μg/ml, Invitrogen) for 2 h at room temperature. Appropriate secondary antibodies labeled with AlexaFluor488 (Invitrogen) were added. Slides were washed with phosphate-buffered saline between incubations and mounted with vectashield containing 4′-6-diamidino-2-phenylindole (Vector, Burlingame, CA).

Quantitative Whole Lysate and Single-Cell PCR

Fibroblasts from two patients with MELAS were grown on glass chamber slides. To determine the total mutation load of the fibroblast cultures, whole extracts were prepared from 10^6 cells harvested after growth in a culture flask. In addition, 50 single cells from each patient were isolated by laser pressure catapulting using a PALM MicroBeam laser microdissection system (PALM/Zeiss, Munich, Germany). DNA was extracted following a published procedure (31), and mtDNA was amplified using 6-FAM labeled forward (5′-CCCACACCCACCCAAGAACA-3′) and NED-labeled backward (5′-TGGCCATGGGTATGTTGTTA-3′) primers with standard reaction mix and conditions (Applied Biosystems, Foster City, CA), and 1.3 units of Hotstar Taq DNA polymerase (Qiagen, Germantown, MD) amplified in 34 cycles. Restriction digest was carried out using 80 IU/μl ApaI (Promega, Madison, WI) for 4 h at 37 °C. The wild-type amplicon does not contain the restriction site generated by the MELAS mutation. Restriction fragments were separated and analyzed by capillary electrophoresis using an ABI3100 genetic Analyzer (Applied Biosystems). Mutation load was calculated by dividing the peak areas of the 6-FAM 41-bp fragment or the NED 75-bp fragment, respectively, by the sum of these peak areas and the corresponding 116-bp wild-type amplicon.

STATEMENT OF FINANCIAL SUPPORT

This study was supported by a grant from the Fund for Scientific Research Belgium (grant G.0666.06). The authors declared no conflict of interest.

REFERENCES

1. Kaim G, Dimroth P. ATP synthesis by F-type ATP synthase is obligatorily dependent on the transmembrane voltage. EMBO J 1999;18:4118–27.
2. Morris AA, Leonard JV, Brown GK, et al. Deficiency of respiratory chain complex I is a common cause of Leigh disease. Ann Neurol 1996;40:25–30.
3. Suomalainen A, Isohanni P. Mitochondrial DNA depletion syndromes–many genes, common mechanisms. Neuromuscul Disord 2010;20:429–37.
4. van den Heuvel L, Smeitink J. The oxidative phosphorylation (OXPHOS) system: nuclear genes and human genetic diseases. Bioessays 2001;23:518–25.
5. Willems PH, Valsecchi F, Distelmaier F, et al. Mitochondrial Ca^{2+} homeostasis in human NADH:ubiquinone oxidoreductase deficiency. Cell Calcium 2008;44:123–33.
6. Valsecchi F, Esseling JJ, Koopman WJ, Willems PH. Calcium and ATP handling in human NADH:ubiquinone oxidoreductase deficiency. Biochim Biophys Acta 2009;1792:1130–7.

7. Carrozzo R, Tessa A, Vázquez-Memije ME, et al. The T9176G mtDNA mutation severely affects ATP production and results in Leigh syndrome. Neurology 2001;56:687–90.
8. Barlan K, Gelfand VI. Intracellular transport: ER and mitochondria meet and greet along designated tracks. Curr Biol 2010;20:R845–7.
9. Barrientos A, Moraes CT. Titrating the effects of mitochondrial complex I impairment in the cell physiology. J Biol Chem 1999;274: 16188–97.
10. Srivastava P, Panda D. Rotenone inhibits mammalian cell proliferation by inhibiting microtubule assembly through tubulin binding. FEBS J 2007;274:4788–801.
11. Tang HL, Lung HL, Wu KC, Le AH, Tang HM, Fung MC. Vimentin supports mitochondrial morphology and organization. Biochem J 2008;410:141–6.
12. Rusanen H, Annunen J, Ylä-Outinen H, et al. Cytoskeletal structure of myoblasts with the mitochondrial DNA 3243A→ G mutation and of osteosarcoma cells with respiratory chain deficiency. Cell Motil Cytoskeleton 2002;53:231–8.
13. Annunen-Rasila J, Ohlmeier S, Tuokko H, Veijola J, Majamaa K. Proteome and cytoskeleton responses in osteosarcoma cells with reduced OXPHOS activity. Proteomics 2007;7:2189–200.
14. Willems PH, Smeitink JA, Koopman WJ. Mitochondrial dynamics in human NADH:ubiquinone oxidoreductase deficiency. Int J Biochem Cell Biol 2009;41:1773–82.
15. Gigarel N, Ray PF, Burlet P, et al. Single cell quantification of the 8993T→G NARP mitochondrial DNA mutation by fluorescent PCR. Mol Genet Metab 2005;84:289–92.
16. Vandewoestyne M, Heindryckx B, Lepez T, et al. Polar body mutation load analysis in a patient with A3243G tRNALeu(UUR) point mutation. Mitochondrion 2011;11:626–9.
17. Budde SM, van den Heuvel LP, Janssen AJ, et al. Combined enzymatic complex I and III deficiency associated with mutations in the nuclear encoded NDUFS4 gene. Biochem Biophys Res Commun 2000;275:63–8.
18. Van Coster R, Seneca S, Smet J, et al. Homozygous Gly555Glu mutation in the nuclear-encoded 70 kDa flavoprotein gene causes instability of the respiratory chain complex II. Am J Med Genet A 2003;120A: 13–8.
19. De Meirleir L, Seneca S, Lissens W, et al. Respiratory chain complex V deficiency due to a mutation in the assembly gene ATP12. J Med Genet 2004;41:120–4.
20. Scalais E, Nuttin C, Seneca S, et al. Infantile presentation of the mitochondrial A8344G mutation. Eur J Neurol 2007;14:e3–5.
21. Seneca S, Goemans N, Van Coster R, et al. A mitochondrial tRNA aspartate mutation causing isolated mitochondrial myopathy. Am J Med Genet A 2005;137:170–5.
22. Meulemans A, Seneca S, Lagae L, et al. A novel mitochondrial transfer RNA(Asn) mutation causing multiorgan failure. Arch Neurol 2006;63:1194–8.
23. Meulemans A, Seneca S, Smet J, et al. A new family with the mitochondrial tRNAGLU gene mutation m.14709T→C presenting with hydrops fetalis. Eur J Paediatr Neurol 2007;11:17–20.
24. Rustin P, Chretien D, Bourgeron T, et al. Biochemical and molecular investigations in respiratory chain deficiencies. Clin Chim Acta 1994;228:35–51.
25. Birch-Machin MA, Shepherd IM, Watmough NJ, et al. Fatal lactic acidosis in infancy with a defect of complex III of the respiratory chain. Pediatr Res 1989;25:553–9.
26. DiMauro S, Servidei S, Zeviani M, et al. Cytochrome c oxidase deficiency in Leigh syndrome. Ann Neurol 1987;22:498–506.
27. Van Coster R, Smet J, George E, et al. Blue native polyacrylamide gel electrophoresis: a powerful tool in diagnosis of oxidative phosphorylation defects. Pediatr Res 2001;50:658–65.
28. De Paepe B, Smet J, Leroy JG, et al. Diagnostic value of immunostaining in cultured skin fibroblasts from patients with oxidative phosphorylation defects. Pediatr Res 2006;59:2–6.
29. Smiley ST, Reers M, Mottola-Hartshorn C, et al. Intracellular heterogeneity in mitochondrial membrane potentials revealed by a J-aggregate-forming lipophilic cation JC-1. Proc Natl Acad Sci USA 1991;88:3671–5.
30. Reers M, Smith TW, Chen LB. J-aggregate formation of a carbocyanine as a quantitative fluorescent indicator of membrane potential. Biochemistry 1991;30:4480–6.
31. Vandewoestyne M, Van Hoofstat D, Van Nieuwerburgh F, Deforce D. Suspension fluorescence in situ hybridization (S-FISH) combined with automatic detection and laser microdissection for STR profiling of male cells in male/female mixtures. Int J Legal Med 2009;123:441–7.